Mixed Convection flow of Chemically reacting Couple Stress fluid in an annulus with Soret and Dufour effects

K. KALADHAR
Department of Mathematics
National Institute of Technology Puducherry
Karaikal- 609 605
INDIA
kkr.nitpy@gmail.com

D. SRINIVASACHARYA
Department of Mathematics
National Institute of Technology Warangal
INDIA
dsrinivasacharya@yahoo.com

Abstract: In this paper, mixed convection flow of couple stress fluid in circular annulus is studied. First order chemical reaction, Soret and Dufour effects are taken into consideration. The governing partial differential equations are transformed into a system of ordinary differential equations and solved by Homotopy Analysis Method (HAM). The effects of Soret number, Dufour number, chemical reaction parameter and couple stress parameter on the dimensionless velocity, temperature and concentration are analyzed graphically.

Key–Words: Mixed convection, Couple stress fluid, Soret and Dufour effects, Chemical reaction, HAM.

1 Introduction

Mixed convection heat transfer and fluid flow in an annulus between two vertical concentric cylinders is the focus of investigation over the past years due to its wide range of practical applications. These applications include electrical machineries where heat transfer occurs in the annular gap between the rotor and stator, growth of single silicon crystals, heat exchangers, cooling systems for electronic devices, solar collectors and other rotating systems [1, 2]. Several studies on the flow between two circular cylinders coupled with heat and mass transfer have appeared in the literature [3, 4, 5]. All the above mentioned attempts describe the flow analysis without chemical reaction.

Chemical reactions can be codified as either heterogeneous or homogeneous processes. This depends on whether they occur at an interface or as a single phase volume reaction. In most cases of chemical reactions, the reaction rate depends on the concentration of the species itself. In many materials processing systems chemical reaction effects may exert a significant role. These include co current buoyant upward gas-liquid flow in packed bed electrodes [6], Sodium Oxide-Silcon dioxide glass melt flows [7], electrochemical generation of elemental bromine in porous electrode systems [8] and the manufacture of intumescent paints for fire safety applications [9]. Further, research on combined heat and mass transfer with chemical reaction and thermophoresis effect can help to design for chemical processing equipment, formation and dispersion of fog, distribution of temperature and moisture over agricultural fields as well as groves of fruit trees, damage of crops due to freezing, food processing, cooling towers, chemically-reactive vapour deposition boundary layers in optical materials processing, catalytic combustion boundary layers, chemical diffusion in disk electrode modeling and carbon monoxide reactions in metallurgical mass transfer and kinetics. Several investigators have examined the effect of chemical reaction on the flow, heat and mass transfer through channels [10, 11], past a flat plate [12, 13, 14] and through concentric cylinders [15].

In all the above studies Soret and Dufour effects are neglected on the basis that they are of a smaller order of magnitude than the effects described by Fourier's and Fick's laws. However, when chemical species are introduced at a surface in fluid domain, with different (lower) density than the surrounding fluid, both Soret (thermo-diffusion) and Dufour (diffusion-thermal) effects can be influential. In combined heat and mass transfer processes, the thermal energy flux resulting from concentration gradients is referred to as the Dufour or diffusion thermal effect. Similarly, the Soret or thermo-diffusion effect is the contribution to the mass fluxes due to temperature gradients. These effects are considered as second order phenomena and may become significant in areas such as hydrology, petrology, geosciences, etc. The Soret effect, for instance, has been utilized for isotope separation and in mixture between gases with very light molecular weight and of medium molecular weight. The Dufour effect was found to be of order of considerable magnitude such that it cannot be ne-

glected [16]. Dursunkaya and Worek [17] studied the diffusion-thermo and thermal-diffusion effects in transient and steady natural convection from a vertical surface, whereas Kafoussias and Williams [18] examined the same effects on mixed convective and mass transfer steady laminar boundary layer flow over a vertical flat plate with temperature dependent viscosity. Several authors have studied the effects and importance of cross diffusion on free convection heat and mass transfers from a vertical surface in a newtonian fluids and non-Newtonian fluids. Awad and Sibanda [19] studied the Dufour and Soret effects on heat and mass transfer in a micropolar fluid in a horizontal channel. Jha and Ajibade [20] considered the Dufour effect on free convection heat and mass transfer flow in a vertical channel.

The study of non-Newtonian fluids has attracted much attention because of their practical applications in engineering and industry, and particularly in the extraction of crude oil from petroleum products. Among these, couple stress fluids introduced by Stokes [21] have distinct features, such as the presence of couple stresses, body couples and non-symmetric stress tensor. The main feature of couple stresses is to introduce a size dependent effect. Classical continuum mechanics neglects the size effect of material particles within the continua. This is consistent with ignoring the rotational interaction among particles, which results in symmetry of the force-stress tensor. However, in some important cases such as fluid flow with suspended particles, this cannot be true and a size dependent couple-stress theory is needed. The spin field due to micro-rotation of freely suspended particles set up an antisymetric stress, known as couple-stress, and thus forming couple-stress fluid. These fluids are capable of describing various types of lubricants, blood, suspension fluids etc. The study of couple-stress fluids has applications in a number of processes that occur in industry such as the extrusion of polymer fluids, solidification of liquid crystals, cooling of metallic plate in a bath, and colloidal solutions etc. Stokes [21] discussed the hydromagnetic steady flow of a fluid with couple stress effects. An excellent treatise on couple stress (polar) fluid dynamics can be seen in [22]. Recently, Srinivasacharya and Kaladhar [23] studied mixed convective flow of couple stress fluid in an annulus with Hall and Ion-Slip effects.

The homotopy analysis method was first proposed by Liao [24] in 1992, is one of the most efficient methods in solving different types of nonlinear equations such as coupled, decoupled, homogeneous and non- homogeneous. Also, HAM provides us a great freedom to choose different base functions to express solutions of a nonlinear problem [25]. The application of the Homotopy Analysis Method (HAM) in engineering problems is highly considered by scientists, because HAM provides us with a convenient way to control the convergence of approximation series, which is a fundamental qualitative difference in analysis between HAM and other methods. Later Liao [26] presented an optimal homotopy analysis approach for strongly nonlinear differential equations. HAM is used to get analytic approximate solutions for heat transfer of a micropolar fluid through a porous medium with radiation by Rashidi et al. [27]. Recent developments of HAM, like convergence of HAM solution, Optimality of convergence control parameter discussed by Srinivasacharya and Kaladhar [28] for the couple stress fluid.

The thermal decomposition of calcium carbonate is a strongly endothermic chemical reaction, forming CO_2 gas. At a higher rate, the reaction must absorb a plenty of heat from the environment and causes a macroscopic volume flux of the product gas from the reaction interface to the main stream. Based on the characteristics mentioned above, the cross-diffusion effect among the chemical reaction, the heat transfer and the mass transfer must be considered during the calcination of limestone when the temperature gradient and the concentration gradient exist simultaneously [29]. Hence, based on the above-mentioned investigations and applications, the present article considers the mixed convection heat and mass transfer flow of a couple stress fluid in an annulus between two circular cylinders with chemical reaction. The Homotopy Analysis method is employed to solve the governing nonlinear equations. Convergence of the derived series solution is analyzed. The behavior of emerging flow parameters on the velocity and temperature is discussed.

2 Mathematical Formulation

Consider a steady, laminar and incompressible couple stress fluid between two coaxial concentric circular cylinders of radii a and b $(a < b)$. Choose the cylindrical polar coordinate system (r, φ, z) with z-axis as the common axis for both cylinders. The inner cylinder is at rest and the outer cylinder is rotating with constant angular velocity Ω. The flow being generated due to the rotation of the outer cylinder. The fluid properties are assumed to be constant except for density variations in the buoyancy force term. In addition, the Soret and Dufour effects with chemical reaction are considered. The flow is a mixed convection, taking place under thermal buoyancy and uniform axial pressure gradient.

With the above assumptions and Boussinesq approximations with energy and concentration, the

equations governing the steady flow of an incompressible couple stress fluid [22] are

$$\frac{\partial u}{\partial \varphi} = 0 \tag{1}$$

$$\frac{\partial p}{\partial r} = \frac{u}{r^2} \tag{2}$$

$$\eta_1 \nabla_1^4 u - \mu \nabla_1^2 u - \rho g \beta_T (T - T_a) + \frac{1}{r}\frac{\partial p}{\partial \varphi} - \rho g \beta_C (C - C_a) = 0 \tag{3}$$

$$\alpha \left[\frac{\partial^2 T}{\partial r^2} + \frac{1}{r}\frac{\partial T}{\partial r}\right] + \frac{D_m K_T}{C_S C_P}\left[\frac{\partial^2 C}{\partial r^2} + \frac{1}{r}\frac{\partial C}{\partial r}\right] + \frac{\mu}{\rho C_P}\left[\left(\frac{\partial u}{\partial r}\right)^2 - 2\frac{u}{r}\frac{\partial u}{\partial r} + \left(\frac{u}{r}\right)^2\right] + \frac{\eta_1}{\rho C_P}(\nabla_1^2 u)^2 = 0 \tag{4}$$

$$D_m \left[\frac{\partial^2 C}{\partial r^2} + \frac{1}{r}\frac{\partial C}{\partial r}\right] + \frac{D_m K_T}{T_m}\left[\frac{\partial^2 T}{\partial r^2} + \frac{1}{r}\frac{\partial T}{\partial r}\right] - k_1 (C - C_a) = 0 \tag{5}$$

where u is the velocity component of the fluid in the direction of φ, p is the pressure, ρ is the density, g is the acceleration due to gravity, μ is the coefficient of viscosity, β_T is the coefficient of thermal expansion, β_C is the coefficient of solutal expansion, α is the thermal diffusivity, D is the mass diffusivity, C_p is the specific heat capacity, C_s is the concentration susceptibility, T_m is the mean fluid temperature, K_T is the thermal diffusion ratio, η_1 is the additional viscosity coefficient which specifies the character of couple-stresses in the fluid, k_1 is the rate of chemical reaction and $\nabla_1^2 u = \dfrac{\partial}{\partial r}\left[\dfrac{1}{r}\dfrac{\partial}{\partial r}(ru)\right]$.

The boundary conditions are given by

$$u = 0 \quad \text{at} \quad r = a, \quad u = b\Omega \quad \text{at} \quad r = b, \tag{6a}$$

$$\nabla_1^2 u = 0 \quad \text{at} \quad r = a \quad \text{and} \quad r = b \tag{6b}$$

$$T = T_a, \quad C = C_a \quad \text{at} \quad r = a \tag{6c}$$

$$T = T_b, \quad C = C_b \quad \text{at} \quad r = b \tag{6d}$$

The boundary condition (6a) corresponds to the classical no-slip condition from viscous fluid dynamics. The boundary condition (6b) imply that the couple stresses are zero at the surfaces.

Introducing the following transformations

$$r = b\sqrt{\lambda}, \quad u = \frac{\Omega}{\sqrt{\lambda}} f(\lambda) \qquad T - T_a = (T_b - T_a)\theta, C - C_a = (C_b - C_a)\phi \tag{7}$$

in equations (3) - (4), we get the following nonlinear system of differential equations

$$S^2\left[\lambda^2 f^{(iv)} + 2\lambda f'''\right] - \frac{1}{4}\lambda f'' - \frac{1}{16}\frac{Gr_T}{Re}\sqrt{\lambda}\theta - \frac{1}{16}\frac{Gr_C}{Re}\sqrt{\lambda}\phi + A = 0 \tag{8}$$

$$\left[\lambda^3\theta'' + \lambda^2\theta'\right] + Br\left[\lambda^2 (f')^2 - 2\lambda f f' + f^2\right] + 4BrS^2\lambda^3\left(f''\right)^2 + PrD_f\left(\lambda^3\phi'' + \lambda^2\phi'\right) = 0 \tag{9}$$

$$\lambda\phi'' + \phi' + S_r Sc\left(\lambda\theta'' + \theta'\right) - \frac{1}{4}KSc\phi = 0 \tag{10}$$

where primes denote differentiation with respect to λ, $Re = \dfrac{\rho\Omega b}{\mu}$ is the Reynolds number, $Pr = \dfrac{\mu C_p}{K_T}$ is the Prandtl number, $Gr_T = \dfrac{\rho^2 g \beta_T b^3}{\mu^2}(T_b - T_a)$ is the temperature Grashof number, $Gr_C = \dfrac{\rho^2 g \beta_C b^3}{\mu^2}(C_b - C_a)$ is the mass Grashof number, $Br = \dfrac{\mu\Omega^2}{(T_b - T_a)K_T}$ is the Brinkman number, $S_r = \dfrac{DK_T(T_b - T_a)}{\nu T_m (C_b - C_a)}$ is the Soret number, $D_f = \dfrac{DK_T(C_b - C_a)}{\nu C_s C_p (T_b - T_a)}$ is the Dufour number, $K = \dfrac{k_1 b^2}{\nu}$ is the chemical reaction parameter, $A = \dfrac{1}{16}\dfrac{b}{\mu\Omega}\dfrac{\partial p}{\partial \varphi}$ is the constant pressure gradient, $S = \dfrac{1}{b}\sqrt{\dfrac{\eta_1}{\mu}}$ is the couple stress parameter, The effects of couple-stress are significant for large values of $\alpha(= l/b)$, where $l = \sqrt{\frac{\eta_1}{\mu}}$ is the material constant. If l is a function of the molecular dimensions of the liquid, it will vary greatly for different liquids. For example, the length of a polymer chain may be a million times the diameter of water molecule [21]. Therefore, there are all the reasons to expect that couple-stresses appear in noticeable magnitudes in liquids with large molecules. where primes denote differentiation with respect to λ,

Boundary conditions (6) in terms of f, θ, ϕ become

$$f = 0, \quad f'' = 0, \quad \theta = 0, \quad \phi = 0 \quad \text{at} \quad \lambda = \lambda_0$$
$$f = b, \quad f'' = 0, \quad \theta = 1, \quad \phi = 1 \quad \text{at} \quad \lambda = 1 \tag{11}$$

where $\lambda_0 = \left(\dfrac{a}{b}\right)^2$.

3 The HAM solution of the problem

For HAM solutions, we choose the initial approximations of $f(\lambda)$, $\theta(\lambda)$ and $\phi(\lambda)$ as follows:

$$f_0(\lambda) = \frac{b}{1-\lambda_0}(\lambda-\lambda_0), \quad \theta_0(\lambda) = \frac{\lambda-\lambda_0}{1-\lambda_0} \quad \phi_0(\lambda) = \frac{\lambda-\lambda_0}{1-\lambda_0} \tag{12}$$

and choose the auxiliary linear operators:

$$L_1 = \frac{\partial^4}{\partial\lambda^4}, \quad L_2 = \frac{\partial^2}{\partial\lambda^2} \tag{13}$$

such that

$$L_1(c_1+c_2\lambda+c_3\lambda^2+c_4\lambda^3) = 0, \quad L_2(c_5+c_6\lambda) = 0. \tag{14}$$

where $c_i (i = 1, 2, ..., 6)$ are constants. Introducing non-zero auxiliary parameters h_1, h_2 and h_3, we develop the zeroth-order deformation problems as follow:

$$(1-p)L_1[f(\lambda;p) - f_0(\lambda)] = ph_1N_1[f(\lambda;p)] \tag{15}$$

$$(1-p)L_2[\theta(\lambda;p) - \theta_0(\lambda)] = ph_2N_2[\theta(\lambda;p)] \tag{16}$$

$$(1-p)L_2[\phi(\lambda;p) - \phi_0(\lambda)] = ph_3N_3[\phi(\lambda;p)] \tag{17}$$

subject to the boundary conditions

$$f(\lambda_0;p) = 0, \quad f''(\lambda_0;p) = 0, \quad f(1;p) = b \quad f''(1;p) = 0, \theta(\lambda_0;p) = 0, \theta(1;p) = 1 \quad \phi(\lambda_0;p) = 0, \quad \phi(1;p) = 1 \tag{18}$$

where $p \in [0,1]$ is the embedding parameter and the non-linear operators N_1, N_2 and N_3 are defined as:

$$N_1[f(\lambda,p),\theta(\lambda,p),\phi(\lambda,p)] = -\frac{1}{4}\lambda f''(\lambda,p) + S^2\left[\lambda^2 f^{(iv)}(\lambda,p) + 2\lambda f'''(\lambda,p)\right] + A - \frac{1}{16}\frac{Gr_T}{Re}\sqrt{\lambda}\theta(\lambda,p) - \frac{1}{16}\frac{Gr_C}{Re}\sqrt{\lambda}\phi(\lambda,p) \tag{19}$$

$$N_2[f(\lambda,p),\theta(\lambda,p),\phi(\lambda,p)] = \lambda^3\theta''(\lambda,p) + \lambda^2\theta'(\lambda,p) + 4BrS^2\lambda^3\left(f''(\lambda,p)\right)^2 + PrD_f\left(\lambda^3\phi''(\lambda,p) + \lambda^2\phi'(\lambda,p)\right) + Br\left[\lambda^2(f')^2 - 2\lambda ff' + f^2\right] \tag{20}$$

$$N_3[f(\lambda,p),\theta(\lambda,p),\phi(\lambda,p)] = \lambda\phi''(\lambda,p) + \phi'(\lambda,p) - \frac{1}{4}KSc\phi(\lambda,p) + S_rSc\left(\lambda\theta''(\lambda,p) + \theta'(\lambda,p)\right) \tag{21}$$

For $p = 0$ we have the initial guess approximations

$$f(\lambda;0) = f_0(\lambda), \theta(\lambda;0) = \theta_0(\lambda), \phi(\lambda;0) = \phi_0(\lambda). \tag{22}$$

When $p = 1$, equations (15) - (17) are same as (8) - (10) respectively, therefore at $p = 1$ we get the final solutions

$$f(\lambda;1) = f(\lambda), \quad \theta(\lambda;1) = \theta(\lambda), \quad \phi(\lambda;1) = \phi(\lambda) \tag{23}$$

Hence the process of giving an increment to p from 0 to 1 is the process of $f(\lambda;p)$ varying continuously from the initial guess $f_0(\lambda)$ to the final solution $f(\lambda)$ (similar for $\theta(\lambda,p)$ and $\phi(\lambda,p)$). This kind of continuous variation is called deformation in topology so that we call system Eqs. (15) - (18), the zeroth-order deformation equation. Next, the mth-order deformation equations follow as

$$L_1[f_m(\lambda) - \chi_m f_{m-1}(\lambda)] = h_1R_m^f(\lambda), \tag{24}$$

$$L_2[\theta_m(\lambda) - \chi_m\theta_{m-1}(\lambda)] = h_2R_m^\theta(\lambda), \tag{25}$$

$$L_2[\phi_m(\lambda) - \chi_m\phi_{m-1}(\lambda)] = h_3R_m^\phi(\lambda), \tag{26}$$

with the boundary conditions

$$f_m(\lambda_0) = 0, f_m(1) = 0, f_m''(\lambda_0) = 0, f_m''(1) = 0 \quad \theta_m(\lambda_0) = 0, \theta_m(1) = 0, \phi_m(\lambda_0) = 0, \phi_m(1) = 0 \tag{27}$$

where

$$R_m^f(\lambda) = S^2\left[\lambda^2 f^{(iv)} + 2\lambda f'''\right] - \frac{1}{4}\lambda f'' - \frac{1}{16}\frac{Gr_T}{Re}\sqrt{\lambda}\theta - \frac{1}{16}\frac{Gr_C}{Re}\sqrt{\lambda}\phi + A(1-\chi_m) \tag{28}$$

$$R_m^\theta(\lambda) = \left[\lambda^3\theta'' + \lambda^2\theta'\right] + 4BrS^2\lambda^3\sum_{n=0}^{m-1} f''_{m-1-n}f''_n + Br\left(\lambda^2\sum_{n=0}^{m-1} f'_{m-1-n}f'_n - 2\lambda\sum_{n=0}^{m-1} f_{m-1-n}f'_n\right) + Br\sum_{n=0}^{m-1} f_{m-1-n}f_n + PrD_f\left(\lambda^3\phi'' + \lambda^2\phi'\right) \tag{29}$$

$$R_m^\phi(\lambda) = \lambda\phi'' + \phi' + S_rSc\left(\lambda\theta'' + \theta'\right) - \frac{1}{4}KSc\phi \tag{30}$$

and, for m being integer

$$\chi_m = 0 \quad \text{for} \quad m \le 1 \qquad = 1 \quad \text{for} \quad m > 1 \tag{31}$$

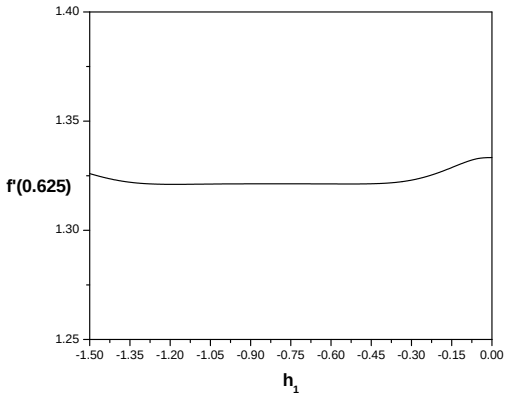

Figure 1: The h curve of $f(\lambda)$ when $D_f = 0.03, S_r = 2.0, S = 1.0, K = 0.1$

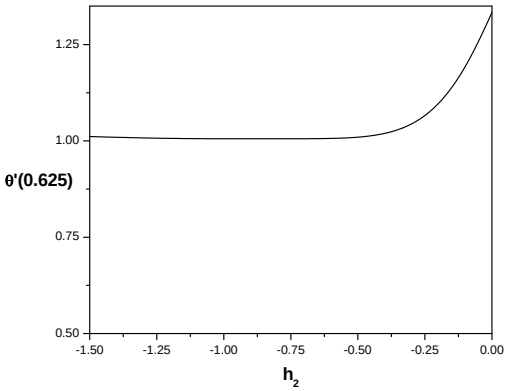

Figure 2: The h curve of $\theta(\lambda)$ when $D_f = 0.03, S_r = 2.0, S = 1.0, K = 0.1$

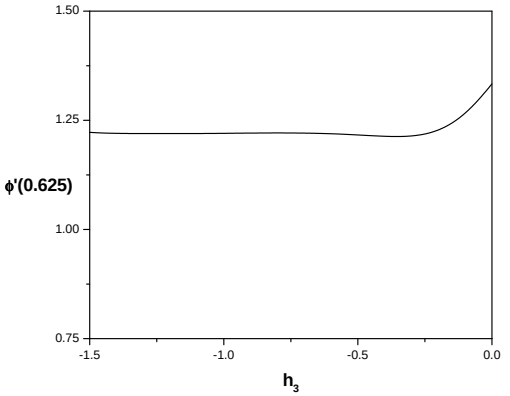

Figure 3: The h curve of $\phi(\lambda)$ when $D_f = 0.03, S_r = 2.0, S = 1.0, K = 0.1$

The initial guess approximations $f_0(\lambda), \theta_0(\lambda)$ and $\phi_0(\lambda)$, the linear operators L_1, L_2 and the auxiliary parameters h_1, h_2 and h_3 are assumed to be selected such that equations (15) - (18) have solution at each point $p \in [0, 1]$ and also with the help of Taylor's series and due to eq. (22); $f(\lambda; p), \theta(\lambda; p)$ and $\phi(\lambda; p)$ can be expressed as

$$f(\lambda; p) = f_0(\lambda) + \sum_{m=1}^{\infty} f_m(\lambda) p^m \tag{32}$$

$$\theta(\lambda; p) = \theta_0(\lambda) + \sum_{m=1}^{\infty} \theta_m(\lambda) p^m \tag{33}$$

$$\phi(\lambda; p) = \phi_0(\lambda) + \sum_{m=1}^{\infty} \phi_m(\lambda) p^m \tag{34}$$

in which h_1, h_2 and h_3 are chosen in such a way that the series (32) - (34) are convergent at $p = 1$. Therefore we have from (23) that

$$f(\lambda; p) = f_0(\lambda) + \sum_{m=1}^{\infty} f_m(\lambda) \tag{35}$$

$$\theta(\lambda; p) = \theta_0(\lambda) + \sum_{m=1}^{\infty} \theta_m(\lambda) \tag{36}$$

$$\phi(\lambda; p) = \phi_0(\lambda) + \sum_{m=1}^{\infty} \phi_m(\lambda) \tag{37}$$

for which we presume that the initial guesses to f, θ and ϕ the auxiliary linear operators L and the non-zero auxiliary parameters h_1, h_2 and h_3 are so properly selected that the deformation $f(\lambda, p)$, $\theta(\lambda, p)$ and $\phi(\lambda, p)$ are smooth enough and their mth-order derivatives with respect to p in equations (35)-(37) exist and are given respectively by $f_m(\lambda) = \frac{1}{m!} \frac{\partial^m f(\lambda; p)}{\partial p^m}\Big|_{p=0}$, $\theta_m(\lambda) = \frac{1}{m!} \frac{\partial^m \theta(\lambda; p)}{\partial p^m}\Big|_{p=0}$, $\phi_m(\lambda) = \frac{1}{m!} \frac{\partial^m \phi(\lambda; p)}{\partial p^m}\Big|_{p=0}$. It is clear that the convergence of Taylor series at $p = 1$, so that the system in (35)-(37) holds true. The formulae in (35)-(37) provide us with a direct relationship between the initial guesses and the exact solutions. All the effects of interaction of the chemical reaction as well as of the heat and mass transfer, Soret and Dufour effects and couple stress flow field can be studied from the exact formulas (35)-(37). Moreover, a special emphasize should be placed here that the mth-order deformation system (24)-(27) is a linear differential equation system with the auxiliary linear operators L whose fundamental solution is known.

4 Convergence of the HAM solution

The expressions for f, θ and ϕ contain the auxiliary parameters h_1, h_2 and h_3. As pointed out by [24], the convergence and the rate of approximation for the HAM solution strongly depend on the values of auxiliary parameter h. For this purpose, h-curves are plotted by choosing h_1, h_2 and h_3 in such a manner that the solutions (32)- (34) ensure convergence [24]. Here to see the admissible values of h_1, h_2 and h_3, the h-curves are plotted for 15th-order of approximation by taking the values of the parameters $Pr = 0.71$, $Sc = 0.22$, $Br = 0.5$, $Re = 2$, $Gr_T = 10$, $Gr_C = 10$, $S = 1.0$, $K = 0.1$, $D_f = 0.03$, $A = 1.0$ and $S_r = 2.0$. It is observed that the admissible values of h_1, h_2 and h_3 are $-1.3 < h_1 < -0.35$, $-1.5 < h_2 < -0.5$ and $-1.5 < h_3 < -0.4$ respectively. To choose optimal value of auxiliary parameter, the average residual errors (see Ref. [26] for more details) are defined as

$$E_{f,m} = \frac{1}{K}\sum_{i=1}^{K}\left(N_1\left[\sum_{j=0}^{m} f_j(i\triangle t)\right]\right)^2 \tag{38}$$

$$E_{\theta,m} = \frac{1}{K}\sum_{i=1}^{K}\left(N_2\left[\sum_{j=0}^{m} \theta_j(i\triangle t)\right]\right)^2 \tag{39}$$

$$E_{\phi,m} = \frac{1}{K}\sum_{i=1}^{K}\left(N_3\left[\sum_{j=0}^{m} \phi_j(i\triangle t)\right]\right)^2 \tag{40}$$

where $\triangle t = 1/K$ and K = 4. At different order of approximations (m), minimum of average residual errors are shown in Tables 1-3. It is clear from Table 1 that the average residual error for f is minimum at $h_1 = -0.8$. It can be seen from Table 2 that the minimum of average residual error for θ attains at $h_2 = -0.8$. Table 3 depicts that at $h_3 = -1.35$, E_θ attains minimum. Therefore, the optimum values of convergence control parameters are taken as $h_1 = -0.8$, $h_2 = -0.8$, $h_3 = -1.35$.

To see the accuracy of the solutions, the residual errors are defined for the system as

$$\begin{aligned} RE_f = {} & S^2\left[\lambda^2 f_n^{(iv)} + 2\lambda f_n'''\right] - \frac{1}{4}\lambda f_n'' \\ & -\frac{1}{16}\frac{Gr_T}{Re}\sqrt{\lambda}\theta_n - \frac{1}{16}\frac{Gr_C}{Re}\sqrt{\lambda}\phi_n + A \end{aligned} \tag{41}$$

$$\begin{aligned} RE_\theta = {} & \left[\lambda^3\theta_n'' + \lambda^2\theta_n'\right] + 4BrS^2\lambda^3\left(f_n''\right)^2 \\ & +Br\left[\lambda^2(f_n')^2 - 2\lambda f_n f_n' + f_n^2\right] \\ & +PrD_f\left(\lambda^3\phi_n'' + \lambda^2\phi_n'\right) \end{aligned} \tag{42}$$

$Order$	$Optimal\,of\,h_1$	$Minimum\,of\,E_m$
10	-0.803	3.25×10^{-5}
15	-0.801	2.87×10^{-6}
20	-0.8	2.35×10^{-7}

Table 1: Optimal value of h_1 at different order of approximations

$Order$	$Optimal\,of\,h_2$	$Minimum\,of\,E_m$
10	-0.79	6.25×10^{-6}
15	-0.8	1.45×10^{-7}
20	-0.8	3.07×10^{-8}

Table 2: Optimal value of h_2 at different order of approximations

$$RE_\phi = \lambda\phi_n'' + \phi_n' + S_rSc\left(\lambda\theta_n'' + \theta_n'\right) - \frac{1}{4}KSc\phi_n \tag{43}$$

where $f_n(\lambda)$, $\theta_n(\lambda)$ and $\phi_n(\lambda)$ are the HAM solution for $f(\lambda)$, $\theta(\lambda)$ and $\phi(\lambda)$. For optimality of the convergence control parameters, residual error [27] for different values of h in the convergence region displayed in Figs. 4-6. We examine that $h_1 = -0.8$, $h_2 = -0.8$, $h_3 = -1.35$ gives a better solution. Table 4 establishes the convergence of the obtained series solution. It is found from the above observations that the series given by (32)-(34) converge in the whole region of λ when $h_1 = -0.8$, $h_2 = -0.8$, $h_3 = -1.35$.

In order to pursue the convergence of the HAM solutions to the exact ones, the graphs for the ratio (following the recent work of [30])

$$\beta_f = \left|\frac{f_m(h)}{f_{m-1}(h)}\right|, \beta_\theta = \left|\frac{\theta_m(h)}{\theta_{m-1}(h)}\right|, \beta_\phi = \left|\frac{\phi_m(h)}{\phi_{m-1}(h)}\right| \tag{44}$$

against the number of terms m in the homotopy series is presented in Figs. 7-9. Figures strongly indicate

$Order$	$Optimal\,of\,h_3$	$Minimum\,of\,E_m$
10	-1.32	3.04×10^{-7}
15	-1.35	6.21×10^{-8}
20	-1.35	6.53×10^{-9}

Table 3: Optimal value of h_3 at different order of approximations

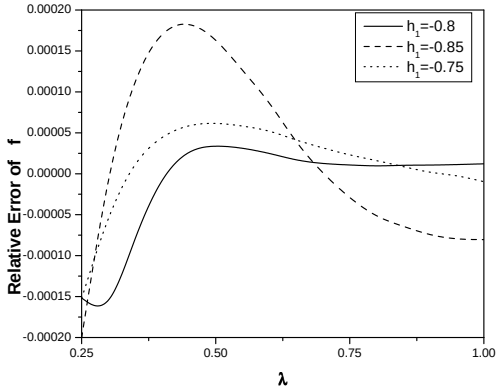

Figure 4: Relative Error of $f(\lambda)$ when $D_f = 0.03, S_r = 2.0, S = 1.0, K = 0.1$

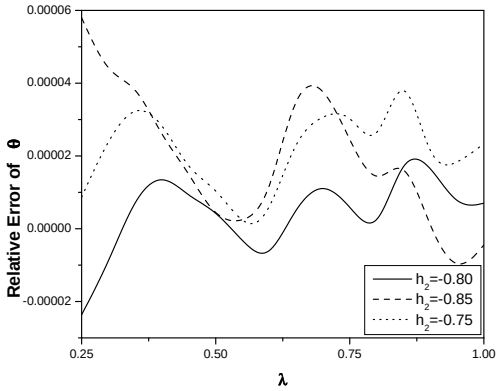

Figure 5: Relative Error of $\theta(\lambda)$ when $D_f = 0.03, S_r = 2.0, S = 1.0, K = 0.1$

that a finite limit of β will be attained in the limit of $m \to \infty$, which will remain less than unity (actually figures imply a limit of 0.92 for f , θ and ϕ). The velocity, temperature and concentration solutions seem to converge in an oscillatory manner requiring more terms in the homotopy series. Thus, the convergence to the exact solution is assured by the HAM method.

5 Results and Discussions

In the absence of Pressure, Buoyancy ratios Gr_T/Re and Gr_C/Re, Eqn. (8) reduces to the equation of motion for the flow between concentric cylinders given in text book by [22]. Analytical solution of that equation with type A conditions and HAM solution at different λ are shown in Table 5. The comparisons are found to be in a very good agreement. Therefore, the HAM code can be used with great confidence to study the

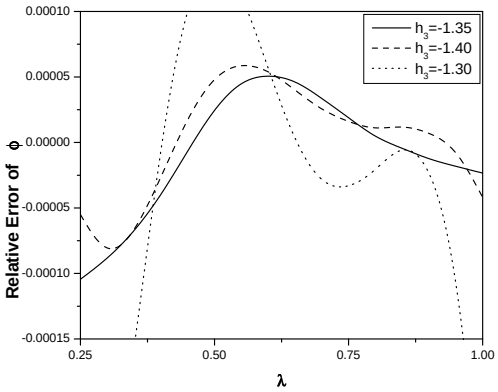

Figure 6: Relative Error of $\phi(\lambda)$ when $D_f = 0.03, S_r = 2.0, S = 1.0, K = 0.1$

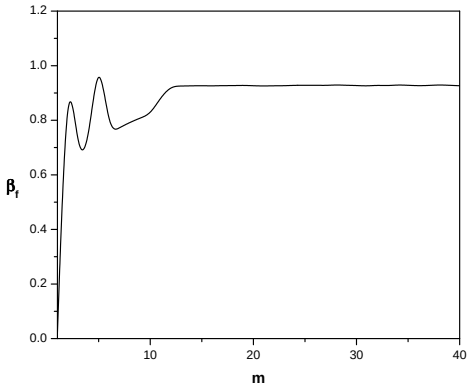

Figure 7: The ratio β_f to reveal the convergence of the HAM solutions

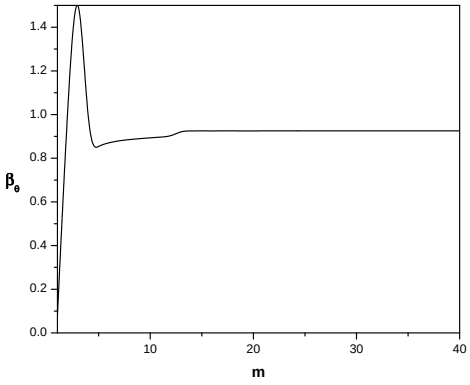

Figure 8: The ratio β_θ to reveal the convergence of the HAM solutions

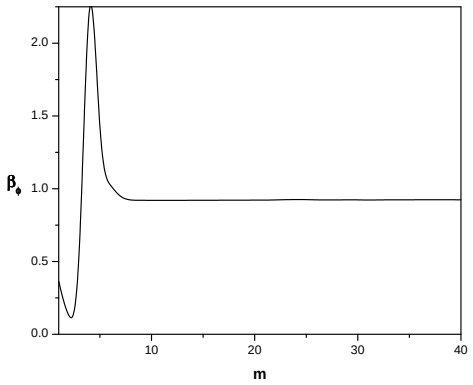

Figure 9: the ratio β_ϕ to reveal the convergence of the HAM solutions

$Order$	$f(0.625)$	$\theta(0.625)$	$\phi(0.625)$
5	0.5428619687252	0.7625482235391	0.6167541586010
10	0.5427881366892	0.7621499292021	0.6161362749928
15	0.5427881329315	0.7621057796564	0.6161362733133
20	0.5427881328643	0.7621056500473	0.6161362733024
30	0.5427881328411	0.7621056500472	0.6161362733023
40	0.5427881328406	0.7621056500471	0.6161362733021
50	0.5427881328402	0.7621056500470	0.6161362733020

Table 4: Convergence of HAM solutions for different order of approximations

	$\alpha = 0.5$	
η	Analytical	HAM
0.5	0.333333	0.333333
0.6	0.466667	0.466667
0.7	0.600000	0.600000
0.8	0.733333	0.733333
0.9	0.866667	0.866667
1.0	1.000000	1.000000

Table 5: Comparison of flow velocity (f) for $A = Gr/Re = 0$

problem considered in this paper.

In order to study the effects of couple stress fluid parameter S, Soret number S_r, Dufour number D_f and Chemical reaction parameter K explicitly. computations were carried out by taking $Pr = 0.71$, $Sc = 0.22$, $Br = 0.5$, $Re = 2$, $Gr_T = 10$, $Gr_C = 10$, $A = 1$. The values of Soret number S_r and Dufour number D_f are chosen in such a way that their product is constant according to their definition provided that the mean temperature T_m is kept constant [18]. These values are used throughout the computations, unless otherwise indicated.

Fig.10 displays the non-dimensional velocity for different values of Soret number S_r and Dufour number D_f with $S = 1.0$ and $K = 0.1$. It is observed from this figure that the velocity of the fluid decreases with the decrease of Dufour number (or increase of Soret number). This is because either a decrease in concentration difference or an increase in temperature difference leads to an increase in the value of the Dufour parameter (D_f). Hence, decreasing the Dufour parameter (D_f) decreases the velocity of the fluid i.e., the lowest peak of the reverse flow velocity corresponds to the highest Soret number and lowest Dufour number. The dimensionless temperature for different values of Soret number S_r and Dufour number D_f with $S = 1.0$ and $K = 0.1$ is shown in Fig.11. It is clear that the temperature of the fluid decreases with the decrease of Dufour number (or increase of Soret number). The parameter S_r (Soret number) does not enter directly into the energy equation and the Dufour effect enhances the mass fluxes and lowers the heat fluxes. Therefore increasing D_f value strongly heats the flow. Fig.12 demonstrates that an increase in Soret number (or decrease of Dufour number) due to the contribution of temperature gradients to species diffusion, increases the concentration.

In Figs. 13-15, the effects of the couple stress parameter S on the dimensionless velocity, temperature and concentration profiles are presented for fixed values of $S_r = 2.0$, $D_f = 0.03$ and $K = 0.1$. As S increases, it is observed from Fig.13 that the maximum velocity increases in amplitude. This happens because of the rotational field of the velocity generated in couple stress fluid. It is clear from Fig. 14 that the temperature increases with the increase of couple stress fluid parameter S. It is seen from Fig.15 that the concentration of the fluid increases with the increase of couple stress fluid parameter S.

Figures 16 to 18 represent the effect of chemical reaction K on $f(\lambda)$, $\theta(\lambda)$ and $\phi(\lambda)$. It is seen from these figures that the velocity $f(\lambda)$ decrease with an increase in the parameter K. The dimensionless temperature decreases as K increases. The concentration $\phi(\lambda)$ decreases with an increase in the parameter K.

Higher values of K amount to a fall in the chemical molecular diffusivity, i.e., less diffusion. Therefore, They are obtained by species transfer. An increase in K will suppress species concentration. The concentration distribution decreases at all points of the flow field with the increase in the reaction parameter. This shows that heavier diffusing species have greater retarding effect on the concentration distribution of the flow field.

An increase in Sc or K will suppress species concentration in the boundary layer regime. Higher Sc will imply a decrease in molecular diffusivity, which comes to a reduction in the concentration boundary layer thickness. Lower Sc will result in higher concentrations, i.e., greater molecular (species) diffusivity causing an increase in concentration boundary layer thickness. The concentration distribution decreases at all points of the flow field with the increase in the Schmidt number and reaction parameter. This shows that heavier diffusing species have greater retarding effect on the concentration distribution of the flow field.

6 Conclusions

In this paper, the Dufour and Soret effects on steady mixed convection of a couple stress fluid between concentric annulus with heat and mass transfer is studied. Using similarity transformations, the governing equations are transformed into non-linear ordinary differential equations. The approximate analytical series solutions are obtained applying homotopy analysis method (HAM).

From the present study we observe that

1. The velocity and the dimensionless temperature of the fluid decreases with the decrease of Dufour number (or increase of Soret number) and with increase of Dufour number (or decrease of Soret number) the concentration of the fluid decreases.

2. The presence of couple stresses in the fluid increases the velocity, temperature and concentration.

3. The velocity, temperature and concentration decreases with the increase in the reaction parameter.

References:

[1] W. Aung, S. Kakac and R. K. Shah. *Handbook of Single-Phase Convective Heat Transfer*, Wiley, New York, Ch. 15, 1987.

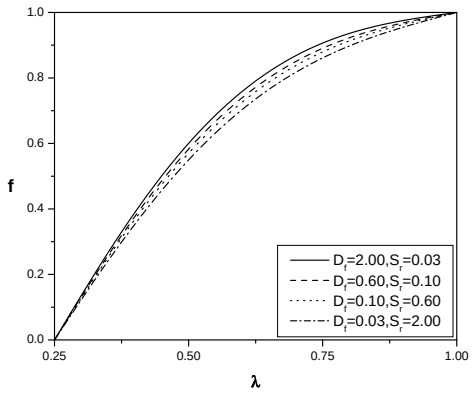

Figure 10: Velocity profile for different values of D_f, S_r at $S = 1.0, K = 0.1$

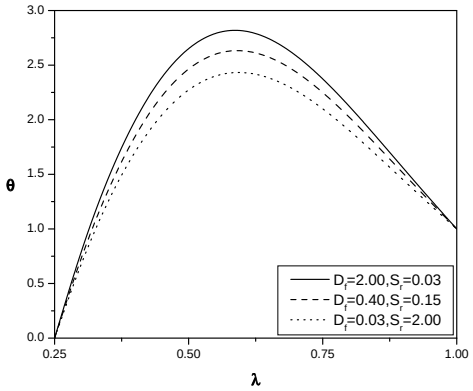

Figure 11: Temperature profile for different values of D_f, S_r at $S = 1.0, K = 0.1$

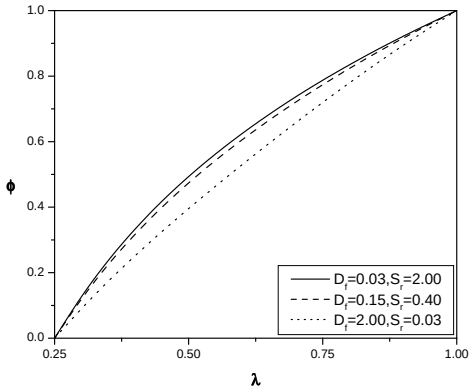

Figure 12: Concentration profile for different values of D_f, S_r at $S = 1.0, K = 0.1$

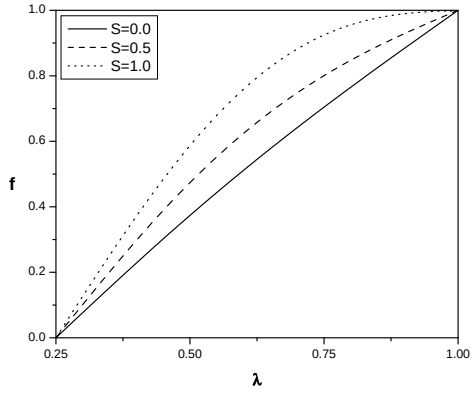

Figure 13: Velocity profile for different values of S at $D_f = 0.03, S_r = 2.0, K = 0.1$

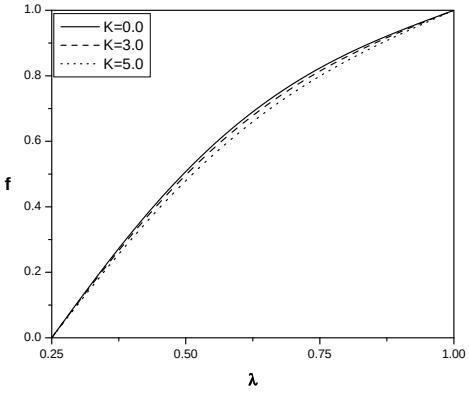

Figure 16: Velocity profile for different values of K at $D_f = 0.03, S_r = 2.0, S = 1.0$

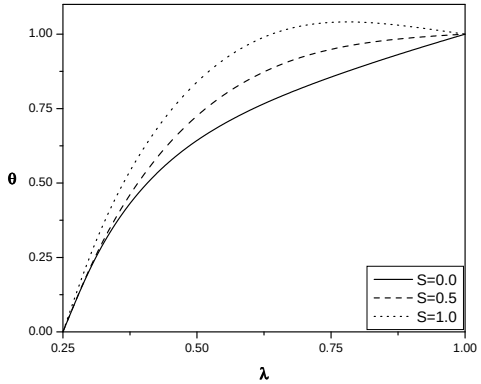

Figure 14: Temperature profile for different values of S at $D_f = 0.03, S_r = 2.0, K = 0.1$

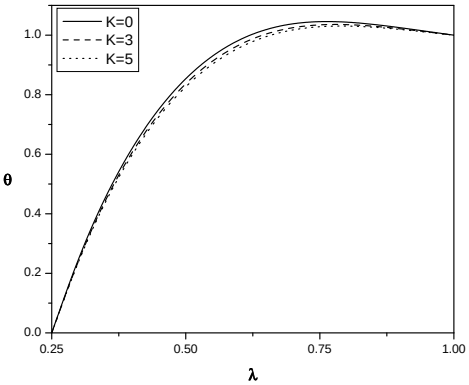

Figure 17: Temperature profile for different values of K at $D_f = 0.03, S_r = 2.0, S = 1.0$

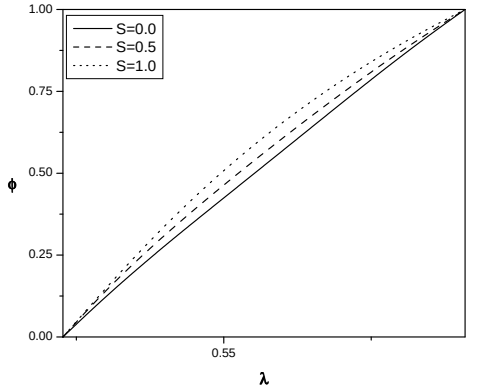

Figure 15: Concentration profile for different values of S at $D_f = 0.03, S_r = 2.0, K = 0.1$

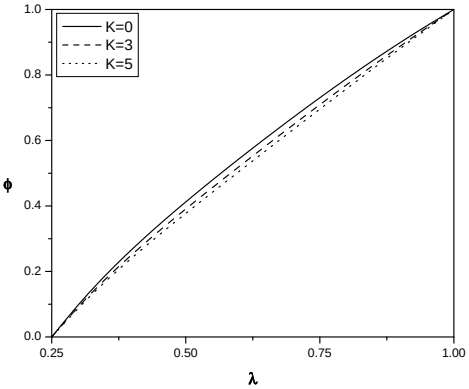

Figure 18: Concentration profile for different values of K at $D_f = 0.03, S_r = 2.0, S = 1.0$

[2] J. D. Jackson, M. A. Cotton and B. P. Axcell, *Int. J. Heat Fluid Flow*, Vol. 10, 1989, pp. 2–15.

[3] D. Maitra and K. Subba Raju, *ASME J. Heat Transfer*, Vol. 97, No. 1, 1997, pp. 135–137.

[4] M. S. Rokerya and M. Iqbal, *Int. J. Heat Mass Transfer*, Vol. 14, 1971, pp. 491–495.

[5] H. S. Kou and D. K. Huang, *Int. Comm. Heat Mass Transfer*, Vol. 24, No. 1, 1997, pp. 99–110.

[6] K. Takahashi and R. Alkire, *Chemical Engineering Communications*, Vol. 38, 1985, pp. 209–227.

[7] Y.A. Guloyan, *Glass and Ceramics*, Vol. 60, 2003, pp. 233-235.

[8] J. Qi and R. F. Savinell, *J. Applied Electrochemistry*, Vol. 23, 1993, pp. 873-886.

[9] P. Ducrocq, S. Duquesne, S. Magnet, S, Bourbigot and R. Delobel, *Progress in Organic Coatings*, Vol. 57, 2006, pp. 430-438.

[10] I. Pop, T. Grosan and R. Cornelia, *Comm. in Nonlinear Sci. and Num. Sim.*, Vol. 15, 2010, pp. 471–474.

[11] S. Shateyi, S. S. Motsa and P. Sibanda, *Can. J. of Chem. Engg.*, Vol. 88, 2010, pp. 975–982.

[12] R. Cortell, *Chemical Engineering and Processing*, Vol. 46, 2007, pp. 721–728.

[13] F. S. Ibrahim, A. M. Elaiw and A.A. Bakr, *Communications in Nonlinear Science Numerical Simulation*, Vol. 13, No. 6, 2008, pp. 1056–1066.

[14] R. A. Damseh and B.A. Shannak, *Appl. Math. Mech.*, Vol. 31, No. 8, 2010, pp. 955-962.

[15] Kermit K. Holman, Sudhir and T. Ashar, *Chemical Engineering Science*, Vol. 26, 1971, pp. 1817–l831.

[16] E. R. G. Eckeret and R. M. Drake, *Analysis of heat and mass transfer*, McGraw Hill, Newyark, 1972.

[17] Z. Dursunkaya and W. M. Worek, *Int. J. Heat Mass Transfer*, Vol. 35, 1992, pp. 2060–2065.

[18] N. G. Kafoussias and N. G. Williams, *Int. J. Engng. Sci.*, Vol. 33, 1995, pp. 1369–1384.

[19] F. Awad and P. Sibanda, *wseas tran. on heat mass transfer*, Vol. 5, No. 3, 2010, pp. 165-177.

[20] B. K. Jha and A. O. Ajibade, *Proc.IMechE, Part E: J. Process mechanical Eng.*, Vol. 224, 2010, pp. 91–101.

[21] V. K. Stokes, *The physics of fluids.,* 1966, pp. 1709–1715.

[22] V. K. Stokes, *Theories of Fluids with Microstructure: An Introduction*, Springer Verlag, New York, 1984.

[23] D. Srinivasacharya and K. Kaladhar, *Turkish J. Eng. Env. Sci.*, Vol. 36, 2012, pp. 226-235.

[24] S. J. Liao, *Beyond perturbation. Introduction to homotopy analysis method.*, Chapman and Hall/CRC Press, and Boca Raton, 2003.

[25] S. J. Liao, *Appl Math Comput.*, Vol. 147, No. 2, 2004, pp. 499–513.

[26] S. J. Liao, *Commun Nonlinear Sci Numer Simulat.*, Vol. 15, 2010, pp. 2003–2016.

[27] M. M. Rashidi, S. A. Mohimanian pour and S. Abbasbandy, *Commun Nonlinear Sci Numer Simulat.*, Vol. 16, 2011, pp. 1874–1889.

[28] D. Srinivasacharya and K. Kaladhar, *Mathematical and Computer Modelling*, Vol. 57, No. 9-10, 2013, pp. 2494–2509.

[29] L. I. Ming-chun, Yan-wen TIAN and Yu-chun ZHAI, *Trans of Nonferrous metals Soc. of China*, Vol. 16, 2006, pp. 1200-1204.

[30] M. Turkyilmazoglu, *Mathematical and Computer Modelling.*, Vol. 53, 2011, pp. 1929–1936.